Fault Reconstruction using a Takagi-Sugeno Sliding Mode Observer for the Wind Turbine Benchmark

Conference Paper · July 2014

DOI: 10.13140/2.1.2959.6808

3 authors:

Florian Pöschke
Hochschule für Technik und Wirtschaft Berlin
2 PUBLICATIONS **2** CITATIONS
SEE PROFILE

Sören Georg
GE Renewable Energy
24 PUBLICATIONS **74** CITATIONS
SEE PROFILE

Horst Schulte
Hochschule für Technik und Wirtschaft Berlin
93 PUBLICATIONS **279** CITATIONS
SEE PROFILE

Fault Reconstruction using a Takagi-Sugeno Sliding Mode Observer for the Wind Turbine Benchmark

Florian Pöschke
TU Clausthal
Inst. of Elec. Power Eng. (IEE)
Clausthal-Zellerfeld,
Germany
Email: florian.poeschke@tu-clausthal.de

Sören Georg
HTW Berlin,
Department of Engineering I,
Control Engineering,
Berlin, Germany,
Email: soeren.georg@htw-berlin.de

Horst Schulte
HTW Berlin,
Department of Engineering I,
Control Engineering,
Berlin, Germany,
Email: schulte@htw-berlin.de

***Abstract*—In this paper, a Takagi-Sugeno sliding mode observer is designed to detect, isolate and reconstruct three different sensor faults and an actuator fault in a specified wind turbine benchmark problem. An extension of the discontinuous observer term using a weighted combination of gains responsible for establishing the sliding motion is proposed. The weights are equivalent to the membership functions of the Takagi-Sugeno (TS) model of the wind turbine. This approach enables new design possibilities for sliding mode observer if the matrices of each local model of the TS model differ significantly. The effectiveness of the design approach is demonstrated by simulation results for fault scenarios defined in the wind turbine benchmark.**

***Index Terms*—Fault diagnosis, fault isolation, sliding mode observer, wind turbines, renewable energy systems**

I. Introduction

Sliding mode observers are used for fault detection and isolation, where actuator or sensor faults are directly reconstructed using the equivalent output injection signal [2]. An important extension to the sliding mode observer concept was presented in [5], where the observer is implemented within a Takagi-Sugeno (TS) model structure to take into account system nonlinearities. In [10], a Takagi-Sugeno sliding mode observer (TS SMO) was successfully applied to detect sensor faults in a dynamic pitch system model of a wind turbine.
A modification of the discontinuous observer term with a weighting matrix for the individual output errors was proposed in [3] by using a gain matrix instead of a scalar gain factor. In this paper, a more extensive modification of the TS SMO from [5], using a weighted combination of gains responsible for establishing the sliding motion, is proposed. The weights are equivalent to the membership functions of the Takagi-Sugeno (TS) model of the wind turbine. This approach enables new design possibilities for sliding mode observer if the matrices of each local model of the TS model differ significantly.
The modified TS SMO is used for the wind turbine benchmark problem in [8], which describes a realistic generic three-blade horizontal variable-speed wind turbine with a full-scale converter coupling. This generic turbine has a rated power of 4.8 MW. Since this model works at the system level, the fast control loops of the converters are not considered. This wind turbine fault detection and isolation (FDI) and fault-tolerant control (FTC) benchmark model was originally presented in [7]. The purpose of this benchmark was to provide a model on which researchers working in the field of fault diagnosis and fault-tolerant control can compare different methods in their field applied to a wind turbine.
This paper is organised as follows. In section II, a brief overview of the modelling of the wind turbine benchmark in Takagi-Sugeno form is given. Section III introduces the idea to modify the TS SMO using a weighted switching term. In section IV, the modified TS SMO is applied to the wind turbine benchmark. The effectiveness of the design approach is demonstrated by simulation results for fault scenarios defined in the benchmark. Finally, in section V these are compared with other results recently summarized in [8].

II. TS Model of the Wind Turbine Benchmark

A. TS Model Structure

Consider a nonlinear MIMO system (1), that is Lipschitz with respect to $\boldsymbol{x}(t) \in \mathbb{R}^n$ and $\boldsymbol{\alpha}(t) \in \mathbb{R}^l$.

$$\begin{aligned} \dot{\boldsymbol{x}}(t) &= \boldsymbol{A}(\boldsymbol{\alpha}(t))\,\boldsymbol{x}(t) + \boldsymbol{B}(\boldsymbol{\alpha}(t))\boldsymbol{u}(t) + \boldsymbol{E}(\boldsymbol{\alpha}(t))\boldsymbol{f}_a(t)\ , \\ \tilde{\boldsymbol{y}}(t) &= \boldsymbol{C}\boldsymbol{x}(t) + \boldsymbol{f}_s(t)\,. \end{aligned} \tag{1}$$

The functions $\boldsymbol{f}_a(t)$ and $\boldsymbol{f}_s(t)$ represent the occuring actuator faults and sensor faults. The output matrix $\boldsymbol{C} \in \mathbb{R}^{p\times n}$ is assumed to be full row rank. It is assumed that the nonlinear model can be represented by a TS system [12] consisting of a fuzzy rule base where each rule $i = 1, \ldots, N_r$ is of the form

Model rule i: IF $(\alpha_1(t)$ is $M_{i1})$ and ... and $(\alpha_l(t)$ is $M_{il})$

$$\text{THEN:} \begin{cases} \dot{\boldsymbol{x}}(t) = \boldsymbol{A}_i\,\boldsymbol{x}(t) + \boldsymbol{B}_i\,\boldsymbol{u}(t) + \boldsymbol{E}_i\,\boldsymbol{f}_a(t)\,, \\ \tilde{\boldsymbol{y}}(t) = \boldsymbol{C}\boldsymbol{x}(t) + \boldsymbol{f}_s(t)\,. \end{cases}$$

where $\alpha_j(t)$ is the jth entry of the premise variables $\boldsymbol{\alpha}(t)$ and M_{ij} is the fuzzy set for the ith model rule and the jth premise variable. The matrices $\boldsymbol{A}_i \in \mathbb{R}^{n\times n}$, $\boldsymbol{B}_i \in \mathbb{R}^{n\times m}$ and $\boldsymbol{E}_i \in \mathbb{R}^{n\times a}$ represent the system dynamics, input gains and gains of the actuator faults. The final fuzzy system with the membership functions $\boldsymbol{h}_i(\alpha(t))$ and N_r rules is inferred as

follows [5]

$$\begin{aligned}\dot{\boldsymbol{x}}(t) &= \sum_{i=1}^{N_r} h_i(\boldsymbol{\alpha}(t))[\boldsymbol{A}_i\boldsymbol{x}(t) + \boldsymbol{B}_i\boldsymbol{u}(t) + \boldsymbol{E}_i\boldsymbol{f}_a] \\ \boldsymbol{y}(t) &= \boldsymbol{C}\boldsymbol{x}(t) + \boldsymbol{f}_s(t)\end{aligned} \tag{2}$$

To construct the TS model the so-called "sector nonlinearity approach" proposed in [12] was used. This method allows to derive an exact representation (globally or at least semi-globally) of a nonlinear system if the nonlinearities $f_k(\boldsymbol{\alpha}(t))$ can be replaced by sector nonlinearities $z_k(\boldsymbol{\alpha}(t))$. The main idea is to derive the TS model by replacing the n_l nonlinear terms of system (1) by the sum of two linear models weighted by nonlinear sector functions $w_{k,1}(\boldsymbol{\alpha}(t))$ and $w_{k,2}(\boldsymbol{\alpha}(t))$, $k = 1, ..., n_l$:

$$f_k(\boldsymbol{\alpha}(t)) = \underline{f}_k \; w_{k,1}(\boldsymbol{\alpha}(t)) + \bar{f}_k \; w_{k,2}(\boldsymbol{\alpha}(t)) \tag{3}$$

with

$$w_{k,1}(\boldsymbol{\alpha}(t)) = \frac{\bar{f}_k - z_k(\boldsymbol{\alpha}(t))}{\bar{f}_k - \underline{f}_k} \tag{4}$$

and

$$w_{k,2}(\boldsymbol{\alpha}(t)) = \frac{z_k(\boldsymbol{\alpha}(t)) - \underline{f}_k}{\bar{f}_k - \underline{f}_k} \tag{5}$$

where $\underline{f}_k := \min(z_k(\boldsymbol{\alpha}(t)))$ and $\bar{f}_k := \max(z_k(\boldsymbol{\alpha}(t)))$. Furthermore, the sector functions satisfy $\sum_{g=1}^{2} w_{k,g}(\boldsymbol{\alpha}(t)) = 1$ and $0 \leq w_{k,g}(\boldsymbol{\alpha}(t)) \leq 1$ for $g = 1, 2$. In a last step, aggregated membership functions $h_i(\boldsymbol{\alpha}(t))$ can be calculated from all combinations of the n_l sector functions $w_{k,g}(\boldsymbol{\alpha}(t))$ [12]. This results in a TS fuzzy model with $n_r = 2^{n_l}$ linear models (rules) of the form (2). Therein, each aggregated model ($\boldsymbol{A}_i$, $\boldsymbol{B}_i$, $\boldsymbol{C}$) represents the system at one combination of the sector bounds and the membership functions $h_i(\boldsymbol{\alpha}(t))$ satisfy $\sum_{i=1}^{n_r} h_i(\boldsymbol{\alpha}(t)) = 1$, $0 \leq h_i(\boldsymbol{\alpha}(t)) \leq 1$.

B. Conversion of the wind turbine model into a TS form

The model of the wind turbine given in [8] leads to a nonlinear state matrix $\boldsymbol{A}(\alpha(t))$, where $\alpha(t) = \frac{\tau_r(t)}{\omega_r(t)}$ is the nonlinear part of the model. $\tau_r(t)$ represents the aerodynamic torque and $\omega_r(t)$ the rotational speed of the rotor.

$$\boldsymbol{A}(\alpha(t)) = \begin{bmatrix} \boldsymbol{A}_{11}(\alpha(t)) & \boldsymbol{0}_{4\times6} \\ \boldsymbol{0}_{6\times4} & \boldsymbol{A}_{22} \end{bmatrix} \tag{6}$$

From $n_l = 1$ nonlinearities, $n_r = 2^{n_l}$ linear models weighted by n_r nonlinear sector functions follow. The bounds $\bar{\alpha}$ and $\underline{\alpha}$ can be found by definition of $\omega_{r,min} = \frac{0.1 \; \frac{rad}{s}}{N_g}$[1], so the nonlinear functions to weigh the linear models can be defined as[2]:

$$h_1(\alpha(t)) = \frac{\alpha(t) - \underline{\alpha}}{\bar{\alpha} - \underline{\alpha}}, \quad h_2(\alpha(t)) = \frac{\bar{\alpha} - \alpha(t)}{\bar{\alpha} - \underline{\alpha}}, \tag{7}$$

where the bounds are

$$\bar{\alpha} = \frac{\rho\pi R^3 C_{q,max} \; v_{w,max}^2}{2 \; \omega_{r,min}} \tag{8}$$

[1]Arbitrary choice such that $\omega_r(t) \geq \omega_{r,min} \forall t$ is satisfied.

[2]Note that in case of $n_l = 1$, it follows that $h_i(\alpha) = w_i(\alpha)$, $i = 1, 2$.

and

$$\underline{\alpha} = \frac{\rho\pi R^3 C_{q,min} \; v_{w,max}^2}{2 \, \omega_{r,min}} \; . \tag{9}$$

$v_{w,max}$ and $\omega_{r,min}$ are used in both of the bounds, since $C_{q,min} < 0$.

$$\boldsymbol{A}_1 = \begin{bmatrix} \boldsymbol{A}_{11,\bar{\alpha}} & \boldsymbol{0}_{4\times6} \\ \boldsymbol{0}_{6\times4} & A_{22} \end{bmatrix}, \quad \boldsymbol{A}_2 = \begin{bmatrix} \boldsymbol{A}_{11,\underline{\alpha}} & \boldsymbol{0}_{4\times6} \\ \boldsymbol{0}_{6\times4} & A_{22} \end{bmatrix} \tag{10}$$

As a result the following TS model is inferred:

$$\begin{aligned}\dot{\boldsymbol{x}}(t) &= \sum_{i=1}^{2} h_i(\alpha(t))[\boldsymbol{A}_i\boldsymbol{x}(t) + \boldsymbol{B}\boldsymbol{u}(t) + \boldsymbol{E}\boldsymbol{f}_a(t)] \\ \boldsymbol{y}(t) &= \boldsymbol{C}\boldsymbol{x}(t) + \boldsymbol{f}_s(t)\end{aligned} \tag{11}$$

III. Takagi-Sugeno Sliding Mode Observer Design

A. Observer structure and existence conditions

The sliding mode concept involves the design of a discontinous feedback ensuring that a sliding surface is reached in finite time and that a sliding motion is maintained. In the majority of works about sliding mode controller and observer design, nominal linear systems are considered. If the nominal system is nonlinear (1), the reconstruction of unknown fault signals may be more difficult due to the large effort necessary to reach and maintain the sliding mode. In order for the proposed Takagi-Sugeno model extension of the sliding mode observer in [2], [13] to exist, the following existence conditions $C1$ to $C3$ have to be fulfilled:

- $C1$ The actuator and sensor faults, as well as the derivatives of the sensor faults are unknown but bounded by Euclidean norms: $\|\boldsymbol{f}_a\| \leq \Xi$, $\|\boldsymbol{f}_s\| \leq \Psi$, $\|\dot{\boldsymbol{f}}_s\| \leq \Psi_d$. Furthermore, the system states $\boldsymbol{x}$ and inputs $\boldsymbol{u}$ are assumed to be bounded.
- $C2$ Let q be defined as the number of columns of the matrices $\boldsymbol{E}_i$. Then, the condition $q = \text{rank}(\boldsymbol{C}\,\boldsymbol{E}_i) = \text{rank}(\boldsymbol{E}_i)$ must be fulfIlled. Furthermore, it must hold that $p > q$, where p is the number of measurable system states.
- $C3$ All invariant zeros of $(\boldsymbol{A}_i, \boldsymbol{E}_i, \boldsymbol{C})$ lie in $\mathbb{C}_-$.

The model equation for the TS SMO based on (2) is

$$\begin{aligned}\dot{\hat{\boldsymbol{x}}}(t) = \sum_{i=1}^{N_r} h_i\left(\boldsymbol{\alpha}(t)\right)\big[&\boldsymbol{A}_i\hat{\boldsymbol{x}}(t) + \boldsymbol{B}_i\boldsymbol{u}(t) \\ &- \boldsymbol{G}_{l,i}\tilde{\boldsymbol{e}}_y(t) + \boldsymbol{G}_{n,i}\boldsymbol{\nu}(t)\big], \\ \hat{\boldsymbol{y}}(t) = \; &\boldsymbol{C}\hat{\boldsymbol{x}}(t)\,,\end{aligned} \tag{12}$$

where $\tilde{\boldsymbol{e}}_y := \hat{\boldsymbol{y}} - \tilde{\boldsymbol{y}}$ denotes the output error and $\boldsymbol{\nu}$ the discontinuous switching term necessary to maintain a sliding motion. The observer gain matrices $\boldsymbol{G}_{l,i}$ and $\boldsymbol{G}_{n,i}$ are obtained from the transformed observer form using a coordinate transformation (see section III-B). The premise variables $\boldsymbol{\alpha}$ in (12) are assumed to be measurable. In [5], a treatment for a TS SMO with unmeasurable premise variables can be found.

B. Transformed form for TS Sliding Mode observer

The sliding mode observer concept by Edwards and Spurgeon makes use of a series of linear coordinate transformations, whereby the underlying system is transformed into $\boldsymbol{z} = \left[\boldsymbol{z}_x^T\,,\,\boldsymbol{z}_y^T\right]^T$, where the measurable system states $\boldsymbol{z}_y \in \mathbb{R}^p$ and the nonmeasurable system states $\boldsymbol{z}_x \in \mathbb{R}^{(n-p)}$ are separated and the actuator faults $\boldsymbol{f}_a$ only influence the change of the measurable states. This separation is achieved by introducing a series of coordinate transformations

$$\boldsymbol{T}_i = \bar{\boldsymbol{T}}_{L,i}\,\tilde{\boldsymbol{T}}_{DE,i}\,\tilde{\boldsymbol{T}}_c\,. \tag{13}$$

The transformation matrices are briefly described in [2], [5]. *Note*: In the following equations, for space reasons, the argument "t" has been omitted. Applying the coordinate transformations (13) to (2) the TS system in transformed form is obtained as

$$\begin{aligned}
\dot{\boldsymbol{z}}_x &= \sum_{i=1}^{N_r} h_i(\boldsymbol{\alpha})\left[\boldsymbol{\mathcal{A}}_{11,i}\,\boldsymbol{z}_x + \boldsymbol{\mathcal{A}}_{12,i}\,\boldsymbol{z}_y + \boldsymbol{\mathcal{B}}_{1,i}\,\boldsymbol{u}\right]\,,\\
\dot{\boldsymbol{z}}_y &= \sum_{i=1}^{N_r} h_i(\boldsymbol{\alpha})\left[\boldsymbol{\mathcal{A}}_{21,i}\,\boldsymbol{z}_x + \boldsymbol{\mathcal{A}}_{22,i}\,\boldsymbol{z}_y + \boldsymbol{\mathcal{B}}_{2,i}\,\boldsymbol{u} + \boldsymbol{\mathcal{E}}_{2,i}\,\boldsymbol{f}_a\right]\,,\\
\boldsymbol{y} &= \boldsymbol{\mathcal{C}}\,\boldsymbol{z} + \boldsymbol{f}_s\,,
\end{aligned} \tag{14}$$

where the transformed system matrices are given by

$$\begin{aligned}
\boldsymbol{\mathcal{A}}_i &= \boldsymbol{T}_i\,\boldsymbol{A}_i\,\boldsymbol{T}_i^{-1} = \begin{bmatrix} \boldsymbol{\mathcal{A}}_{11,i} & \boldsymbol{\mathcal{A}}_{12,i} \\ \boldsymbol{\mathcal{A}}_{21,i} & \boldsymbol{\mathcal{A}}_{22,i} \end{bmatrix},\\
\boldsymbol{\mathcal{B}}_i &= \boldsymbol{T}_i\,\boldsymbol{B}_i = \begin{bmatrix} \boldsymbol{\mathcal{B}}_{1,i} \\ \boldsymbol{\mathcal{B}}_{2,i} \end{bmatrix},\\
\boldsymbol{\mathcal{C}} &= \boldsymbol{C}\,\boldsymbol{T}_i^{-1} = \left[\boldsymbol{0}_{p\times(n-p)}\;\boldsymbol{I}_p\right],\\
\boldsymbol{\mathcal{E}}_i &= \boldsymbol{T}_i\,\boldsymbol{E}_i\,.
\end{aligned}$$

The system in transformed form (14) will be used to design the TS sliding mode observer

$$\begin{aligned}
\dot{\hat{\boldsymbol{z}}}_x &= \sum_{i=1}^{N_r} h_i(\boldsymbol{\alpha})[\boldsymbol{\mathcal{A}}_{11,i}\,\hat{\boldsymbol{z}}_x + \boldsymbol{\mathcal{A}}_{12,i}\,\hat{\boldsymbol{z}}_y + \boldsymbol{\mathcal{B}}_{1,i}\,\boldsymbol{u} - \boldsymbol{\mathcal{A}}_{12,i}\,\tilde{\boldsymbol{e}}_y]\\
\dot{\hat{\boldsymbol{z}}}_y &= \sum_{i=1}^{N_r} h_i(\boldsymbol{\alpha})[\boldsymbol{\mathcal{A}}_{21,i}\hat{\boldsymbol{z}}_x + \boldsymbol{\mathcal{A}}_{22,i}\hat{\boldsymbol{z}}_y + \boldsymbol{\mathcal{B}}_{2,i}\boldsymbol{u}\,,\\
&\quad - (\boldsymbol{\mathcal{A}}_{22,i} - \boldsymbol{\mathcal{A}}_{22}^s)\,\tilde{\boldsymbol{e}}_y + \boldsymbol{\nu}]\\
\hat{\boldsymbol{y}} &= \boldsymbol{\mathcal{C}}\hat{\boldsymbol{z}}\,,
\end{aligned} \tag{15}$$

with $\boldsymbol{\mathcal{A}}_{22}^s$ as a stable design matrix. The vector $\boldsymbol{\nu}$ is defined by

$$\boldsymbol{\nu} = \begin{cases} -\left(\sum\limits_{i=1}^{N_r} h_i(\boldsymbol{\alpha})\,\boldsymbol{\rho}_i\right)\frac{\mathbf{P}_2\,\boldsymbol{W}\,\tilde{\boldsymbol{e}}_y}{\|\mathbf{P}_2\,\boldsymbol{W}\,\tilde{\boldsymbol{e}}_y\| + \delta} & \text{if } \tilde{\boldsymbol{e}}_y \neq \boldsymbol{0} \\ \boldsymbol{0} & \text{otherwise} \end{cases}, \tag{16}$$

where $\boldsymbol{\rho} = \mathrm{diag}(\rho_1 \cdots \rho_p)$ is a diagonal, positive definite gain matrix. The weighting matrix $\boldsymbol{W}$ is a positive definite, diagonal matrix consisting of the reciprocal values of the estimated maximum absolute values of the output vector components: $\boldsymbol{W} = \mathrm{diag}\,(W_1 \cdots W_p) = \mathrm{diag}\left(\frac{1}{|\boldsymbol{y}_1|_{\max}} \cdots \frac{1}{|\boldsymbol{y}_p|_{\max}}\right)$. $\boldsymbol{P}_2$ is the unique symmetric positive definite (s.p.d) solution of the Lyapunov equation $\boldsymbol{P}_2\,\boldsymbol{\mathcal{A}}_{22}^s + \boldsymbol{\mathcal{A}}_{22}{}^T\,\boldsymbol{P}_2 = -\boldsymbol{Q}_2$, where $\boldsymbol{Q}_2$ is a symmetric positive definite design matrix. Once the sliding surface $\mathcal{S} = \{\boldsymbol{e}\,(t) \in \mathbb{R}^n : \tilde{\boldsymbol{e}}_y = \boldsymbol{0}\}$ is reached, the observer tries to maintain the sliding motion on $\mathcal{S}$.

In addition to the fault and uncertainty bounds in existence condition 1, the error vector $\boldsymbol{e}_1 = \hat{\boldsymbol{x}}_1 - \boldsymbol{x}_1$ of the unmeasurable states is assumed to be bounded $\|\boldsymbol{e}_1\| < \Gamma$, which was considered in [5] and is omitted here for the sake of brevity. For a unique $\boldsymbol{\rho} = \boldsymbol{\rho}_i\ \forall i$, the design steps and the existence condition for a sliding motion were given in [3] where it was shown that the TS SMO using the modified switching term (16) is able to establish an ideal sliding motion in finite time if the following condition is fulfilled:

$$\tilde{\boldsymbol{e}}_y^T\left[\left(\boldsymbol{\rho} - \mathcal{K}_{\max}\,\boldsymbol{I}_{p\times p}\right)\left(\boldsymbol{P}_2\boldsymbol{W}\right)^2\right]\tilde{\boldsymbol{e}}_y > \boldsymbol{0}\,, \tag{17}$$

where $\mathcal{K}_{\max}$ is given by with Ψ_d as the upper bound $\left\|\dot{\boldsymbol{f}}_s\right\|$ $\mathcal{K}_{\max} := \|\boldsymbol{\mathcal{A}}_{21}\|_{\max}\,\Gamma + \|\boldsymbol{\mathcal{A}}_{22}\|_{\max}\,\Psi + \|\boldsymbol{\mathcal{E}}_2\|_{\max}\,\Xi + \Psi_d$. The extension in (16) with the weighted sum of $\boldsymbol{\rho}_i$ is presented here for the first time. A proof of the existence condition for an ideal sliding motion can be obtained by following along the lines of the proof in [3]. The existence condition in (17) is then simply replaced by

$$\tilde{\boldsymbol{e}}_y^T\left[\left(\boldsymbol{\rho}_i - \mathcal{K}_i\,\boldsymbol{I}_{p\times p}\right)\left(\boldsymbol{P}_2\boldsymbol{W}\right)^2\right]\tilde{\boldsymbol{e}}_y > \boldsymbol{0}\,, \tag{18}$$

where $\mathcal{K}_i$ is given by $\mathcal{K}_i := \|\boldsymbol{\mathcal{A}}_{21,i}\|\,\Gamma + \|\boldsymbol{\mathcal{A}}_{22,i}\|\,\Psi + \|\boldsymbol{\mathcal{E}}_{2,i}\|\,\Xi + \Psi_d$. *Note*: The weighted switching term (16) was first introduced in [3] to achieve good simultaneous reconstruction of fault signals in systems were the orders of magnitude of the outputs differ significantly. In the case of wind turbines, this is the case for the two control signals, the pitch angle and the generator torque, which are also included as system states and outputs in the model equations.

C. Actuator and sensor fault reconstruction

For fault reconstruction, the discontinuous switching term (16) is replaced by a continuous approximation:

$$\boldsymbol{\nu}_{eq} = -\left(\sum_{i=1}^{N_r} h_i(\boldsymbol{\alpha})\,\boldsymbol{\rho}_i\right)\frac{\mathbf{P}_2\,\boldsymbol{W}\,\tilde{\boldsymbol{e}}_y}{\|\mathbf{P}_2\,\boldsymbol{W}\,\tilde{\boldsymbol{e}}_y\| + \delta}\,, \tag{19}$$

with a small positive constant δ. The equivalent output injection signal $\boldsymbol{\nu}_{\text{eq}}$ describes the average behaviour of the discontinuous term (16). If no sensor faults are present, actuator faults can be reconstructed using the relation

$$\hat{\boldsymbol{f}}_a = \left(\sum_{i=1}^{N_r} h_i\,(\boldsymbol{\alpha})\,\boldsymbol{\mathcal{E}}_{2,i}\right)^+ \boldsymbol{\nu}_{\text{eq}} \qquad [2], [5] \tag{20}$$

On the other hand, if no actuator faults are presented sensor faults can be reconstructed using the relation

$$\hat{\boldsymbol{f}}_s = \left(\mathscr{A}(\boldsymbol{\alpha}(t))\right)^+ \boldsymbol{\nu}_{\text{eq}} \tag{21}$$

where $^+$ denotes the pseudo inverse and $\mathscr{A}(\boldsymbol{\alpha}(t))$ is

$$\mathscr{A}(\boldsymbol{\alpha}(t)) = -\Big(\sum_{i=1}^{N_r} h_i(\boldsymbol{\alpha}(t))\, \boldsymbol{\mathcal{A}}_{22,i} - \sum_{i=1}^{N_r} h_i(\boldsymbol{\alpha}(t))\, \boldsymbol{\mathcal{A}}_{21,i} \Big[\sum_{i=1}^{N_r} h_i(\boldsymbol{\alpha}(t))\, \boldsymbol{\mathcal{A}}_{11,i} \Big]^{-1} \sum_{i=1}^{N_r} h_i(\boldsymbol{\alpha}(t)) \boldsymbol{\mathcal{A}}_{22,i} \Big) .$$

Hint: In a strict mathematical sense, the existence of the pseudo inverse in (20),(21) is not guaranteed yet. However, it could be shown by the following numeric results, that the pseudo inverse could be determined in each iteration step.

D. Choice of the gain matrices and weighting matrices

As a starting point, the allowed common lower bound of the gains $\boldsymbol{\rho}_i$ [2] are chosen. Then, each value was iteratively determined to satisfy the fault detection, isolation and reconstruction requirements of the benchmark. The following gain matrices $\boldsymbol{\rho}_{1,2}$ and weighting matrix $\boldsymbol{W}$ were determined:

$$\boldsymbol{\rho}_1 = \text{diag}[\, 3 \cdot 10^3,\, 7.5 \cdot 10^3,\, 1 \cdot 10^7,\, 1 \cdot 10^4,\, 1 \cdot 10^4,\, 1 \cdot 10^4 \,],$$

$$\boldsymbol{\rho}_2 = \text{diag}[\, 1 \cdot 10^3,\, 7.5 \cdot 10^3,\, 1 \cdot 10^7,\, 1 \cdot 10^4,\, 1 \cdot 10^4,\, 1 \cdot 10^4 \,],$$

and

$$\boldsymbol{W} = \text{diag}\Big[\, \frac{1}{1.4},\, \frac{1}{20},\, \frac{1}{4000},\, \frac{1}{5},\, \frac{1}{5},\, \frac{1}{5} \,\Big] .$$

IV. Simulation results

The TS SMO solution is able to detect and isolate the faults 1, 2, 3, 6, 7 and 8. In addition to the detection and isolation it is possible to reconstruct faults[3] 1, 2, 3 and 8 to a certain degree of accuracy. The denotation $\hat{f}_{fil}$ in a signal name results from the fact, that there exists a non filtered reconstructed signal $\hat{f}$ and a filtered reconstructed signal. Sensor noise is defined by the benchmark and considered in the simulation. The reconstructed signals of the faults are based on the noisy signals of the benchmark, which show a noisy behaviour as well. This is handled by the use of a filter. From the filtered reconstructed fault signals a detection signal is generated, which depends on the thresholds defined in section V.
The designed observer can not differentiate between actuator faults and sensor faults. Since the wind turbine benchmark provides two sensors per output, two observers can be used, which work in parallel and have the same structure. When a sensor fault occurs, only one observer notices a faulty behaviour of the benchmark. By contrast, actuator faults have an influence on both observers. With respect to that fact the differentiation between sensor and actuator faults can be achieved by the use of two observers.
Since the detection signals are based on reconstructed fault signals, the fault detection signal changes its state when the reconstructed fault signals drop under a certain threshold (e.g. cf. Fig. 5 and 6).

[3]The bias of some reconstructed signals are caused by δ, which has the effect of a continuous approximation of ν and is than called ν_{eq} . This leads to a slight bias from the sliding surface.

A. Fault 1

In the time period from 2000 to 2100 s, the measurement of the pitch angle $\beta_{1,m1}$ remains on a fixed value of 5° [8]. Since the reference pitch position β_r remains on a value of 0°, the fault in the measurement stays on a constant value of 5°. Fig. 1 shows the detection signal of the fault and Fig. 2 shows the reconstructed signal of the fault $\hat{f}_{s,4,fil}$. A reconstruction accuracy of ≈ 94 % is reached (cf. Fig 2).

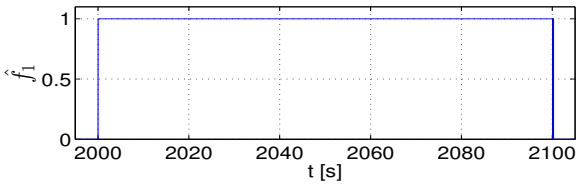

Fig. 1. Fault 1: Detection signal $\hat{f}_1$

B. Fault 2

In the time period from 2300 to 2400 s, a gain factor equal to 1.2 on $\beta_{2,m2}$ occurs [8]. The detection of the fault with the presented TS SMO solution is possible only if the pitch position is $\neq \beta_2$. Since the pitch system's reference position β_r is equal to 0 until $t \approx 2310\ s$, the required detection time of $T_D \leq 0.1\ s$ cannot be reached (cf. Fig. 3). The reconstruction of the fault, which occurs resulting from a gain factor on $\beta_{2,m2}$, can be seen in Fig. 4. In Fig. 4 the real resulting fault signal $f_{s,5}$ is compared to the reconstructed fault signal $\hat{f}_{s,5,fil}$, which shows a good accuracy of reconstruction. The detection signal oscillates because of the fault characteristic. Since the magnitude of the occurring sensor fault depends on the state of the pitch position, the sensor fault signal can fall under the defined threshold when the pitch position is small (cf. Fig. 3).

C. Fault 3

In the time period from 2600 to 2700 s, the measurement of the pitch angle $\beta_{3,m1}$ remains on a fixed value of 10° [8]. The fault detection signal can be seen in Fig. 5. The reconstructed fault $\hat{f}_{s,6,fil}$ signal is compared to the real resulting fault signal $f_{s,6}$ in Fig. 6 and shows a good accuracy of reconstruction. The magnitude of the fault $f_{s,6}$ changes depending on the faultless pitch position of the plant. When the magnitude undercuts the defined threshold, the detection signal can switch its state, cf. Fig. 5.

D. Fault 6

In the time period from 2900 to 3000 s, the pitch actuator 2 works with changed dynamics due to hydraulic pressure drop [8]. Since the measurement of the pitch rate is not given in the benchmark model, a reconstruction with the presented TS SMO solution is not provided. The reconstruction of the parameter faults under consideration of the pitch rate was shown in [4]. The detection of fault 6 is based on an artificial actuator fault modelled in the form $\dot{\beta}_2(t) = \dot{x}_8(t) = x_7(t) + f_{a,4}(t)$.

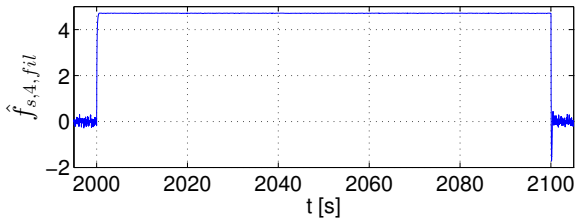

Fig. 2. Fault 1: Reconstructed signal $\hat{f}_{s,4,fil}$

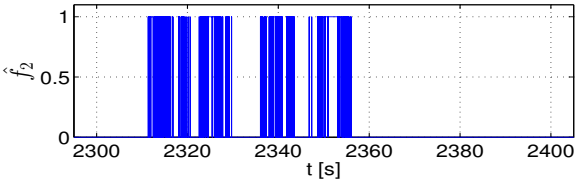

Fig. 3. Fault 2: Detection signal $\hat{f}_2$

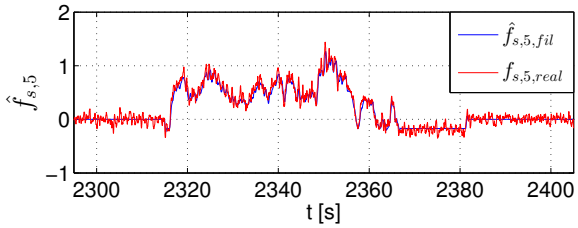

Fig. 4. Fault 2: Reconstructed signal $\hat{f}_{s,5,fil}$

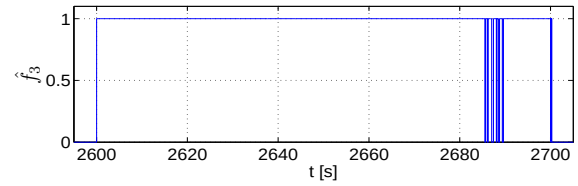

Fig. 5. Fault 3: Detection signal $\hat{f}_3$

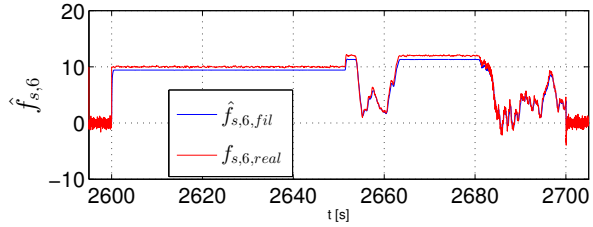

Fig. 6. Fault 3: Reconstructed signal $\hat{f}_{s,6,fil}$

The detection signal can be seen in Fig. 7. The pitch system is modelled as a second-order lag element, whose stationary gain equals 1 and thus is in stationary state invariant to parameter faults. This leads to the oscillation of the detection signal.

E. Fault 7

In the time period from 3500 to 3600 s, the pitch actuator 3 works with changed dynamics due to increased air content

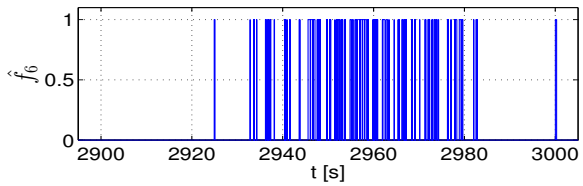

Fig. 7. Fault 6: Detection signal $\hat{f}_6$

in the oil [8][4]. Since the measurement of the pitch rate is not given in the benchmark model, a reconstruction with the presented TS SMO solution is not provided. The detection of fault 7 is based on an artificial actuator fault modelled in the form $\dot{\beta}_3(t) = \dot{x}_{10}(t) = x_9(t) + f_{a,5}(t)$. The detection signal can be seen in Fig. 8. The reason for the oscillation of the detection signal equals the explanation in Fault 6.

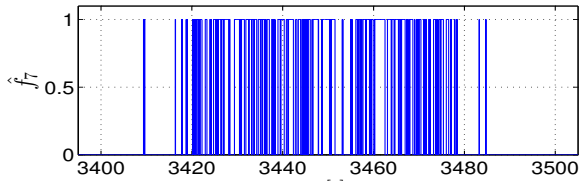

Fig. 8. Fault 7: Detection signal $\hat{f}_7$

F. Fault 8

In the time period from 3800 to 3900 s, an offset of 100 Nm on τ_g occurs. Fig. 9 shows the detection signal of the fault and Fig. 10 shows the reconstructed signal of the fault $\hat{f}_{s,4,fil}$. A reconstruction accuracy of ≈ 96 % is reached (cf. Fig. 10).

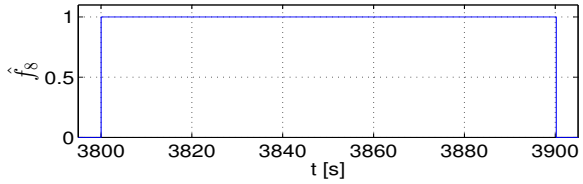

Fig. 9. Fault 8: Detection signal $\hat{f}_8$

V. Comparison of the FDI Solutions

The following thresholds were chosen for the detection of the faults: FD Threshold Fault 1 = 0.6°, FD Threshold Fault 2 = 0.6°, FD Threshold Fault 3 = 0.6°, FD Threshold Fault 6 = 5, FD Threshold Fault 7 = 5, FD Threshold Fault 8 = 10 Nm.

For the TS SMO solution Monte Carlo studies were not applied yet. Thus, the resulting times of the simulation are compared to the mean value of detection time of the other solutions:

[4]In the given benchmark model the fault is implemented in the time period from 3400 to 3500 s.

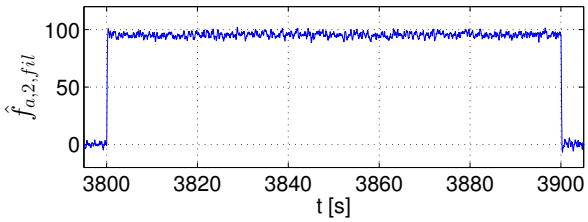

Fig. 10. Fault 8: Reconstructed signal $\hat{f}_{a,2,fil}$

TABLE I
DETECTION TIME: FAULTS 1,2 AND 3

Solution	$\bar{T}_d[s]$ Fault 1	$\bar{T}_d[s]$ Fault 2	$\bar{T}_d[s]$ Fault 3
GKSV	**0.02**	47.24	**0.02**
EB	**0.02**	44.65	0.54
UDC	**0.03**	69.12	**0.04**
COK	10.32	19.24	10.35
GFM	**0.04**	13.70	**0.05**
TS SMO	**0.022**	11.375	**0.017**

- GKSV: Gaussian Kernel SVM Solution [6]
- EB: Estimation-Based Solution [14]
- UDC: Up-Down Counter-based Solution [9]
- COK: Combined Obs. and Kalman Filter Solution [1]
- GFM: General Fault Model Solution [11]

The bold time values in Tab. II, III and IV fulfill the requirements given by the benchmark. With the exception of Fault 4 and Fault 5 the TS SMO is able to detect all faults which the other solutions were able to handle. The detection times are in the range of other presented solutions.

VI. CONCLUSION

In this paper, a Takagi-Sugeno sliding mode observer (TS SMO) was used to detect, isolate and reconstruct sensor and actuator faults in a wind turbine benchmark. The benchmark model simulates the actuator, sensor, and system faults in the pitch actuators, drive train, and converter system. Nine different faults were included in this test bench model, with different time locations of the faults, which corresponded to different operating points at which the faults occurred.
The fault detection, isolation and reconstruction module in this system was designed based on a Takagi-Sugeno sliding mode observer. The FDI scheme described herein allows for successful detection and identification of six of nine faults. In addition, the dynamics of Fault 1,2 and 3 are reconstructed from the equivalent output injection signal of the TS SMO. Finally, all simulation results were compared with the previously published results [1], [6], [9], [11], [14] in terms of the mean detection time $\bar{T}_d$ of each fault. The main advantage of the TS SMO is the possibility to reconstruct faults in addition to the detection and isolation.

TABLE II
DETECTION TIME: FAULTS 4,5 AND 6

Solution	$\bar{T}_d[s]$ Fault 4	$\bar{T}_d[s]$ Fault 5	$\bar{T}_d[s]$ Fault 6
GKSV	0.11	25.90	-
EB	0.33	**0.01**	11.31
UDC	**0.02**	2.96	11.81
COK	0.18	31.32	23.80
GFM	**0.10**	9.49	15.52
TS SMO	-	-	24.948

TABLE III
DETECTION TIME: FAULTS 7,8 AND 9

Solution	$\bar{T}_d[s]$ Fault 7	$\bar{T}_d[s]$ Fault 8	$\bar{T}_d[s]$ Fault 9
GKSV	-	**0.01**	-
EB	26.07	**0.01**	-
UDC	12.93	**0.02**	-
COK	34.00	**0.01**	-
GFM	31.70	7.92	-
TS SMO	9.350	0.038	-

REFERENCES

[1] W. Chen, S. X. Ding, A. H. A. Sari, A. Naik, A. Q. Khan, and S. Yin, Observer-based FDI schemes for wind turbine benchmark, in *Proc. IFAC World Congr.*, Aug.–Sep. 2011, pp. 7073–7078.

[2] C. Edwards, S.K. Spurgeon, Sliding Mode Control: Theory and Applications, Taylor & Francis, Boca Raton, 1998.

[3] S. Georg, H. Schulte, "Takagi-Sugeno Sliding Mode Observer with a Weighted Switching Action and Application to Fault Diagnosis for Wind Turbines," in Józef Korbicz and Marek Kowal (eds.), *Intelligent Systems in Technical and Medical Diagnostics*, vol. 230 of Advances in Intelligent Systems and Computing, pp. 41-52, Springer-Verlag Berlin Heidelberg, 2014.

[4] S. Georg, H. Schulte, "Diagnosis of Actuator Parameter Faults in Wind Turbines using a Takagi-Sugeno Sliding Mode Observer," in Józef Korbicz and Marek Kowal (eds.), *Intelligent Systems in Technical and Medical Diagnostics*, vol. 230 of Advances in Intelligent Systems and Computing, pp. 29-40, Springer-Verlag Berlin Heidelberg, 2014.

[5] P. Gerland, D. Gross, H. Schulte, and A. Kroll, "Design of Sliding Mode Observers for TS Fuzzy Systems with Application to Disturbance and Actuator Fault Estimation," in *Proc. IEEE International Conference on Decision and Control*, Atlanta, USA, Dec. 2010, pp. 4373–4378.

[6] N. Laouti, N. Sheibat-Othman, and S. Othman, Support vector machines for fault detection in wind turbines, in *Proc. IFAC World Congr.*, Aug.–Sep. 2011, pp. 7067–7072.

[7] P. F. Odgaard, J. Stoustrup, and M. Kinnaert, Fault tolerant control of wind turbines: A benchmark model," in Proc. *7th IFAC Symp. Fault Detection, Supervis., Safety Tech. Process.*, Jul. 2009, pp. 155–160.

[8] P. F. Odgaard, J. Stoustrup, and M. Kinnaert, "Fault-Tolerant Control of Wind Turbines: A Benchmark Model," *IEEE Transactions on Control Systems Technology*, vol. 21. no. 4, pp. 1168–1182, July 2013.

[9] A. A. Ozdemir, P. Seiler, and G. J. Balas, Wind turbine fault detection using counter-based residual thresholding, in *Proc. IFAC World Congr.*, Aug.–Sep. 2011, pp. 8289–8294.

[10] H. Schulte, M. Zajac, S. Georg, "Takagi-Sugeno Sliding Mode Observer Design for Load Estimation and Sensor Fault Detection in Wind Turbines", in *Proc. IEEE International Conference on Fuzzy Systems*, Brisbane, Australia, June 2012, pp. 292–299.

[11] C. Svard and M. Nyberg, Automated design of an FDI-system for the wind turbine benchmark, in *Proc. IFAC World Congr.*, Aug.–Sep. 2011, pp. 8307–8315.

[12] Tanaka, K., Wang, H.O.: Fuzzy Control Systems Design and Analysis: A Linear Matrix Inequality Approach. John Wiley & Sons, Inc., 2001.

[13] X. Yan and C. Edwards, "Nonlinear robust fault reconstruction and estimation using a sliding mode observer," *Automatica*, vol. 43, no. 9, pp. 1605–1614, 2007.

[14] X. Zhang, Q. Zhang, S. Zhao, R. M. G. Ferrari, M. M. Polycarpou, and T. Parisini, Fault detection and isolation of the wind turbine benchmark: An estimation-based approach, in *Proc. IFAC World Congr.*, Sep. 2011, pp. 8295–8300.